Soft Matter

Cite this: *Soft Matter*, 2012, **8**, 4216

www.rsc.org/softmatter

PAPER

Short-ranged pair distribution function for concentrated suspensions of soft particles

Lavanya Mohan and Roger T. Bonnecaze*

Received 12th October 2011, Accepted 13th January 2012
DOI: 10.1039/c2sm06940g

Many rheological properties of concentrated suspensions of soft particles jammed together beyond the random close packing limit for hard-spheres are determined by the contacts between the particles and are computable from the short range value of the pair distribution function. It is a challenge to compute the structure of these amorphous suspensions because they are athermal, non-equilibrium materials. Here we develop a microscopic theory to predict the short ranged pair distribution function with a transport or conservation of mass equation for the stationary state that includes a concentration dependent mean force that captures the effect of the bulk suspension on the pair interaction. The resulting distribution function is singular as the concentration approaches random close packing as expected from the theory for hard spheres. The pair distribution function and elastic properties that can be calculated from it are validated by computer simulations and experiments with concentrated suspensions of particles with varying soft potentials.

1. Introduction

Concentrated suspensions of soft particles are useful as rheological modifiers for food, cosmetics, organic inks and coatings. They possess both solid- and liquid-like characteristics. At rest, they behave like elastic solids, and they are typically shear-thinning when continuously deformed. These disordered suspensions consist of deformable and impenetrable particles jammed beyond the random close packing fraction for hard spheres ($\phi_c = 0.64$).[1] Examples include microgel suspensions,[2,3] polymer coated colloids[4], and compressed oil in water emulsions.[5] The dispersed particle sizes in these jammed systems range from a few nanometres[6] to hundreds of micrometres.[4] The elasticity of the particles is derived from surface tension, osmotic or entropic/steric forces, depending on their composition.[7] Despite the different particle sizes and sources of elasticity, these concentrated suspensions of soft particles share many common properties.[7,8]

In these suspensions it is the elastic repulsion forces that are dominant and not the thermal forces thus they are referred to as athermal. The microstructural and rheological properties of these materials are determined by the contacts between the particles. The high packing fraction leads to particles pushing against each other and forming an elastic cage of contacts around each particle.[3,6,9,10] In the stationary state when the particle distribution function becomes time independent, the elastic interactions among the particles determines their microstructure. Given the microstructure embodied by the pair distribution function, the bulk elastic properties of these concentrated suspensions can be determined, *e.g.*, the high frequency modulus *via* the Zwanzig-Mountain relationship.[11] Since the interaction potentials between soft particles often vanish beyond contact, only the short-ranged pair distribution function (at radial separations less than a particle diameter) is needed to compute their bulk properties.

The athermal nature, ultrasoft interactions and high packing fractions make theoretical determination of the microstructure of these concentrated suspensions of soft particles a challenge. Theories to predict the pairwise distribution function of systems of hard spheres have been developed extensively.[12,13] In the case of soft particles, several closure relationships have been coupled with the Ornstein-Zernike relation[14–17] to obtain the pairwise distribution function. Hard sphere perturbation theories have been developed for the same, where equivalent diameters with respect to hard sphere systems are chosen based on matching the free energies,[18–23] Boltzmann factors,[24] liquid structure factors[25] or second virial coefficients[26] of the system. However, these methods are only applicable at volume fractions below random close packing, where a hard sphere reference states exists. Further, the temperature factor or thermal energy that plays a major role in these theories is not significant in the case of the soft particle suspensions examined here, where the elastic interactions due to the large compressions are dominant, again making it difficult or impossible to apply these theories in practice for highly concentrated, athermal suspensions of soft particles.

In this paper we develop a microscopic theory to predict the radial pair distribution function $g(r)$ that describes the structure

Department of Chemical Engineering and Texas Materials Institute, The University of Texas at Austin, Austin, Texas, 78712, USA. E-mail: rtb@che.utexas.edu

of these amorphous, jammed systems. The constituent particles are impenetrable and form flat facets at contact and the behavior at these facets determine the properties of these materials. Elastic properties of the soft particle glasses, such as the osmotic pressure and high frequency modulus can be determined from the pairwise radial distribution function.[11,13] Further, since interaction potentials between soft particles vanish beyond contact, only the distribution function resolved over a short range is needed. In Section 2 we describe a pairwise theory to compute the radial pair distribution function. Particle scale simulations and the insights gained from them are discussed in Section 3. Theoretical predictions of the short ranged pair distribution function and the elastic properties that can be calculated from it are presented in Section 4. The theory is validated by comparison with data from computer simulations and experiments. Finally, because the particles are impenetrable, the pair distribution function should diverge at random close packing. The nature of the divergence of contact value of g(r) at random close packing has also been studied and the predictions from our theory agree well with previously published results.

2. Theory

Consider a reference particle located at the origin surrounded by a suspension of compressed soft particles as shown in Fig. 1. The constituent particles being deformable as well as impenetrable form flat facets (indicated by the dark colored contact regions) at contact in high concentration suspensions. The probability of finding a test particle located at r is proportional to the pair distribution function $g(r)$, which we would like to determine in order to compute the elastic properties of the concentrated suspension of soft particles. The transport or conservation equation for the pair distribution function is given by,[27]

$$\nabla\cdot[g(r)\mathbf{V}(r)] = 0, \tag{1}$$

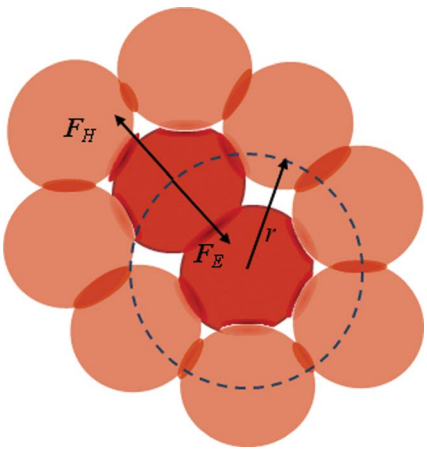

Fig. 1 (Color online). Schematic of forces acting on a test particle located a distance r from the reference particle. The radial pair distribution function $g(r)$ is determined by the transport eqn (1). The forces acting on a particle (dark red) a distance r from the reference particle (dark red at origin) are the pairwise contact force F_H and the effective many body force of the concentrated suspension surrounding the particle F_E. These forces are balanced at the stationary state and determine pair distribution function. The darker contact regions represent the flat facets formed due to the impenetrable nature of particles.

where $\mathbf{V}(r)$ is the velocity of the test particle, located at r, relative to the reference particle due to elastic forces of all the particles. We imagine the velocity of the test particle to be the result of two contributions: the pairwise elastic interaction with the reference particle and the effect of all the other particles surrounding it. Thus, $\mathbf{V}(r) = \mathbf{M}\cdot[\mathbf{F}_H + \mathbf{F}_E]$, where $\mathbf{M}$ is the mobility of the particles. Although the eqn (1) is expressed in terms of the net flux of the pair distribution function, we may still use it to determine the stationary state of the system by considering the point where the net flux or $\mathbf{V}(r)$ vanishes, which will occur when $\mathbf{F}_H = -\mathbf{F}_E$.

The pairwise elastic repulsion between the test particle and the reference particle is given by

$$\mathbf{F}_H(r) = -\frac{du(r)}{dr}\mathbf{e}_r, \tag{2}$$

where $u(r)$ is the interaction potential between the particles and $\mathbf{e}_r$ is the radial unit vector. $\mathbf{F}_E$ is the sum of the forces or the effective mean elastic force of all the other particles surrounding the test particle except for the reference particle. Since the reference particle is excluded, this force will act in the opposite direction of $\mathbf{F}_H$, thus providing the balancing force at the stationary state. We postulate this many body force is the sum of the negative pairwise elastic force $-\mathbf{F}_H(r_m)$, where r_m is the radius of maximum pairwise density (separation between particles where $\frac{dg(r)}{dr} = 0$), and a force analogous to the Brownian force in thermal systems,[28] so that,

$$\mathbf{F}_E(r) = -\mathbf{F}_H(r_m) - \langle U\rangle\nabla\ln g(r), \tag{3}$$

where the thermal energy kT is replaced by the average elastic energy $\langle U\rangle$. This average elastic energy depends on the pairwise interaction potential and increases with increasing volume fraction ϕ. The rationale for this postulate is that at r_m the many body force on the test particle must balance the force on the test particle due to the reference particle, hence the first term in eqn (3). In addition to the analogy to a Brownian force, the second term in eqn (3) may be considered a potential of the mean force acting on the test particle. The average energy $\langle U\rangle$ is used as the prefactor because it is the natural energy scale for this system of particles that only interact with one another elastically.

At the stationary state (no flow) the pair distribution function of the suspension is radially symmetric, and thus eqn (1) becomes

$$\frac{d}{dr}\left[r^2 g(r)\left(F_H(r) - F_H(r_m) - \langle U\rangle\frac{d\ln g(r)}{dr}\right)\right] = 0, \tag{4}$$

where the scalar function $F_H(r) = -\frac{du(r)}{dr}$.Note that the mobility drops out and thus its value is not needed for the remaining analysis. Because the potential vanishes beyond contact, eqn (4) is only valid for radial positions less than the particle diameter and so only describes the short-ranged pair distribution function. However, only the short-ranged value is needed to compute the bulk properties of the suspension. From the integration of eqn (4) and the fact that the $g(r)$ is finite and continuous, it is found that

$$g(r) = a(\phi)\exp\left[-\frac{1}{\langle U\rangle}[u(r) + F_H(r_m)(r - r_m)]\right]. \tag{5}$$

What remains is the determination of the three constants, $\langle U \rangle$, a and r_m, all of which depend on volume fraction. They are determined by the following conditions. First, the average energy $\langle U \rangle$ is proposed to be the energy per contact per particle and is determined self-consistently using the relationship,

$$\langle U \rangle = \frac{\int_0^{2R} 4\pi n r^2 u(r) g(r) dr}{2\int_0^{2R} 4\pi n r^2 g(r) dr}. \quad (6)$$

The factor of two in the denominator is included because each contact is shared between two particles. Second, the number of contacts per particle N is also constrained so that

$$N = \int_0^{2R} 4\pi n r^2 g(r) dr. \quad (7)$$

It has been found that $N = N_c + K_N(\phi - \phi_c)^v$, where $N_c = 6$ is the number of contacts at random close packing, $K_N = 7.7 \pm 0.5$ and $v = 0.5 \pm 0.03$.[29,30] The constraint on the number of contacts is useful in determining the coefficient $a(\phi)$ in eqn (5). Finally, the non-dimensional overlap distance $2 - r_m/R$ has been observed to follow the scaling $K_r(N - N_c)$[21,31] A preliminary estimate for K_r can be obtained by the following mass conservation argument. Consider a random close packing of spheres with radius R_{rcp} in a fixed volume V. Imagine the particle radius being increased to R such that the final volume fraction is unity. The final radius R would be $R_{rcp}\phi_c^{-1/3}$. Assuming that the spheres were just touching each other at random close packing, the overlap distance $2 - r_m/R$ at the final volume fraction is thus given by $\frac{2}{R}(R - R_{rcp}) = 2(1 - \phi_c^{1/3})$. Comparing this to the scaling for the overlap distance and the relationship between number of contacts and volume fraction already available, we find that $K_r \cong 0.013$. Thus, using the scaling for r_m in eqn (5), and self consistently determining $\langle U \rangle$ using eqn (6), and $a(\phi)$ using eqn (7), we can determine the short-range pair distribution function for any given volume fraction and interaction potential.

Given the short-range pair distribution function, the osmotic pressure π of the suspensions may be determined according to[13]

$$\pi = -\frac{4\pi n^2}{6}\int_0^{2R} r^3 g(r)\frac{du(r)}{dr} dr, \quad (8)$$

and the high-frequency modulus G_∞ can be computed with the Zwanzig-Mountain formula[11]

$$G_\infty = \frac{2\pi}{15} n^2 \int_0^{2R} g(r)\frac{d}{dr}\left[r^4 \frac{du(r)}{dr}\right] dr \quad (9)$$

In the next section the constants $\langle U \rangle$ and a are evaluated by numerical integration.

It is insightful to develop an approximate analytical expression of $g(r)$ as follows. For r close to r_m, $u(r)$ can be written as the Taylor-series expansion

$$u(r) = u(r_m) + u'(r_m)(r - r_m) + \frac{u''(r_m)}{2}(r - r_m)^2 + O\left((r - r_m)^3\right). \quad (10)$$

Using this approximation up to the quadratic term in eqn (5), we find the pair distribution to have the Gaussian form[32]

$$\begin{aligned} g(r) &= a(\phi)\exp\left[-\frac{1}{\langle U \rangle}\left[u(r_m) + \frac{u''(r_m)}{2}(r - r_m)^2\right]\right], \\ &= g_0(\phi)\exp\left[-\frac{u''(r_m)}{2\langle U \rangle}(r - r_m)^2\right]. \end{aligned} \quad (11)$$

where

$$g_0(\phi) = a(\phi)\exp\left[-\frac{u(r_m)}{\langle U \rangle}\right]. \quad (12)$$

The constant $a(\phi)$ and thus $g_0(\phi)$ are determined by the constraint on the number of contacts in eqn (7). Using the form of $g(r)$ in eqn (11), $a(\phi)$ is determined to be given by

$$a(\phi) = \frac{N}{4\pi n I}\exp\left[\frac{u(r_m)}{\langle U \rangle}\right] \quad (13)$$

where

$$\begin{aligned} I = \frac{\delta^2}{2}\exp\left(-\frac{(4 + r_m{}^2)}{\delta^2}\right)\left[\exp\left(\frac{4}{\delta^2}\right)r_m - \exp\left(\frac{4r_m}{\delta^2}\right)(2 + r_m)\right] \\ + \frac{\sqrt{\pi}\delta^3}{4}\left(1 + \frac{2r_m{}^2}{\delta^2}\right)\left[\mathrm{erf}\left(\frac{r_m}{\delta}\right) - \mathrm{erf}\left(\frac{(r_m - 2)}{\delta}\right)\right] \end{aligned} \quad (14)$$

and

$$\delta = \sqrt{\frac{2\langle U \rangle}{u''(r_m)}} \quad (15)$$

is the width of the peak of $g(r)$. The peak value $g_0(\phi)$ can be determined from $a(\phi)$ using eqn (12).

In general the pairwise interaction potential depends on the overlap, say $u(r) \sim (2 - r)^\lambda$, where λ is some positive exponent. The average elastic energy $\langle U \rangle \sim u(r_m) \sim (2 - r_m)^\lambda$. And $u''(r_m)$ is the second derivative of the interaction potential and scales as $(2 - r_m)^{\lambda - 2}$. This makes $\delta \sim (2 - r_m)$. The overlap $(2 - r_m) \sim (N - N_c)^2 \sim (\phi - \phi_c)$ as indicated previously. Thus, the width of the peak scales as $\delta \sim (\phi - \phi_c)$.

3. Particle scale computer simulations

Particle scale simulations were done to validate the predictions from theory for three different interparticle potentials. The pair distribution functions, osmotic pressure and the shear moduli were computed using the methodology described elsewhere in detail[32] and briefly recapitulated here. To create highly concentrated packings of soft spheres, three-dimensional, periodically replicated random close packed configurations of hard spheres were first generated using the compression algorithm introduced by Lubachevsky and Stillinger.[33] After forming the close-packed, hard-sphere microstructure, the spheres were treated as soft particles. Each close packed configuration was compressed by reducing the box size in small decrements until the desired concentration was achieved. After each decrement, the system is allowed to relax using a conjugate gradient algorithm to minimize the system energy or equivalently ensure the net contact forces on each particle vanish. These configurations were used to compute the pair distribution function, π and G_∞. The three pairwise interaction potentials are listed in Table 1 for Hertzian contacts for linearly elastic spheres, the potential for a compressed emulsions and the potential for spheres composed

Table 1 Pairwise interaction potentials used in simulations

Interaction potential	$u(r)$	Parameters
Hertz potential[32,34]	$\frac{8}{15\sqrt{2}}E^*R^3\left(2-\frac{r}{R}\right)^{2.5}$	E^* – particle contact modulus, R – particle radius
Compressed emulsions[35]	$2\gamma R^2 C\left(\left(\frac{2R}{r}\right)^3-1\right)^{\alpha}$	γ – interfacial tension, $C=0.36$, $\alpha=2.32$
Mooney-Rivlin material[36]	$\frac{4}{3\sqrt{2}}\frac{C'}{n+1}E^*R^3\left(2-\frac{r}{R}\right)^{n+1}$	$C'=1$, $n=1.5$ for $r/R>1.9$ $C'=31.62$, $n=3$ for $1.8<r/R<1.9$ $C'=790.57$, $n=5$ for $r/R>1.8$

of a non-linear elastic Mooney-Rivlin material. The pairwise elastic repulsion force for these interaction potentials is presented in Fig. 2.

The simulations confirm that $N = N_c + K_N(\phi - \phi_c)^{1/2}$ where $N_c = 6$, $\phi_c = 0.64$ and $2 - r_m/R = K_r(N - N_c)$. The constants K_N and K_r were found to depend slightly on the nature of the interacting potential. They were found to be very close to the values in literature and our preliminary estimate cited earlier. Fig. 3 shows the effect of volume fraction and interaction potential on the number of contacts and overlap at r_m, respectively. The effect of the interaction potential is more evident at higher volume fractions as the particles are more compressed and the interaction energy is more important. The average energies $\langle U \rangle$ from simulations match very closely the self consistently determined values from theory. The agreement between theoretical predictions and simulation values are shown in Fig. 4a. The average elastic energy vanishes as we move towards the random close packing limit as shown in Fig. 4b, a necessary condition for the pair distribution function to become singular at $\phi_c = 0.64$.

4. Results and discussion

Fig. 5 shows the theoretical predictions of the radial distribution functions computed using eqn (5) with the three constraints discussed and their comparison to simulation results. Calculations were done with three different pairwise interaction potentials for linear elastic Hertzian spheres, compressed emulsions, and non-linear elastic Mooney-Rivlin spheres as given in Table 1. Appropriate values of K_N and K_r were used for each interaction potential. Unlike concentrated hard sphere suspensions, the centers between soft particles can be less than two radii apart. The results have been shown for volume fractions 0.675, 0.7, 0.75, 0.8, 0.85 and 0.9 in the insets and for volume fractions of 0.7, 0.8 and 0.9 in the main figures. Indeed the peak sharpens and narrows as the volume fraction approaches that for hard spheres at random close packing. This transition is shown most clearly, for example, in Fig. 5d for the Hertz potential.

For the Hertz potential and compressed emulsions, the peak of $g(r)$ decreases while the spread increases with increase in volume fraction. For a given volume fraction, the spread of the curve is lower for stiffer potentials. In the case of the Mooney-Rivlin material at $\phi = 0.90$, compressions > 20% become more likely and the interaction at these compressions becomes stiffer which leads to a narrower $g(r)$ curve with a larger peak. The theoretical predictions closely match the results from simulations and thus validate the theory.

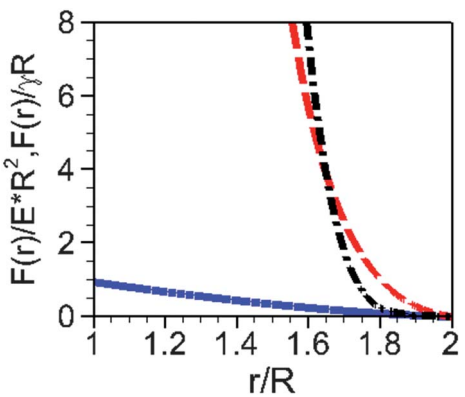

Fig. 2 (Color Online) Elastic Repulsion forces for hertz potential (solid lines), compressed emulsion potential (dashed) and Mooney-Rivlin material potential (dash-dot).

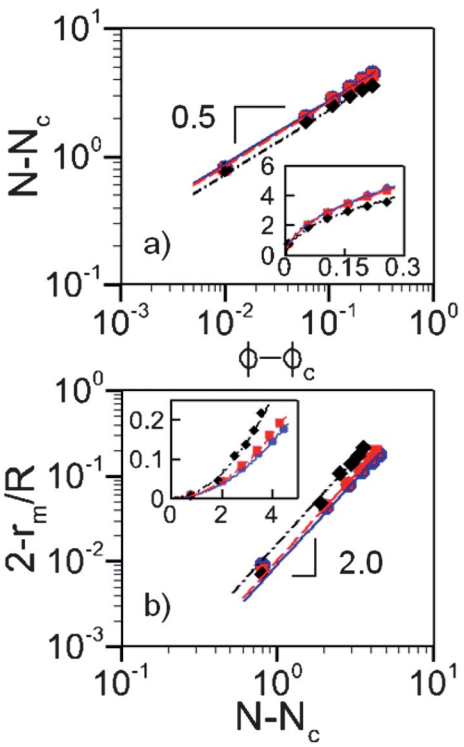

Fig. 3 (Color online) Simulation results (symbols) and corresponding models for $N - N_c$(a) and $2 - r_m/R$(b). Lines: fits with scaling laws using constants $K_r = 0.0091$, 0.0105, 0.016 and $K_N = 8.67$, 8.49, 7.31 for Hertz (circles), compressed emulsions (squares) and Mooney-Rivlin materials (diamonds), respectively. Insets: linear scale.

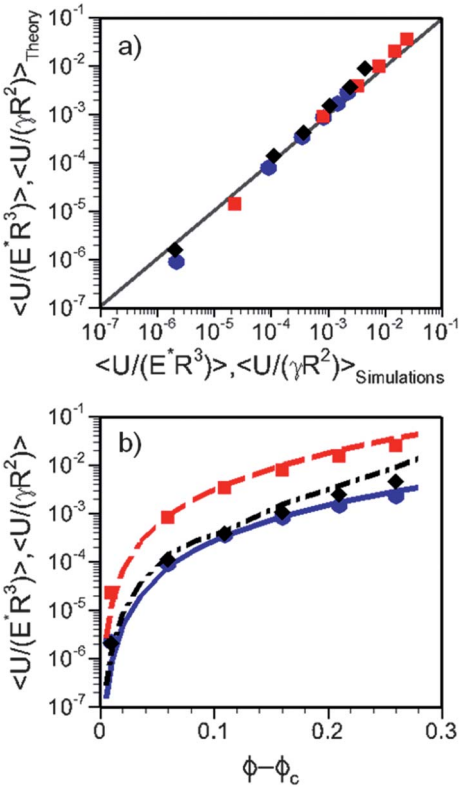

Fig. 4 (Color online) a) Comparison of theoretical predictions (lines) of average elastic energy with simulation results (symbols). b) Variation of average energy with volume fraction for Hertz (circles), compressed emulsions (squares) and Mooney-Rivlin materials (diamonds).

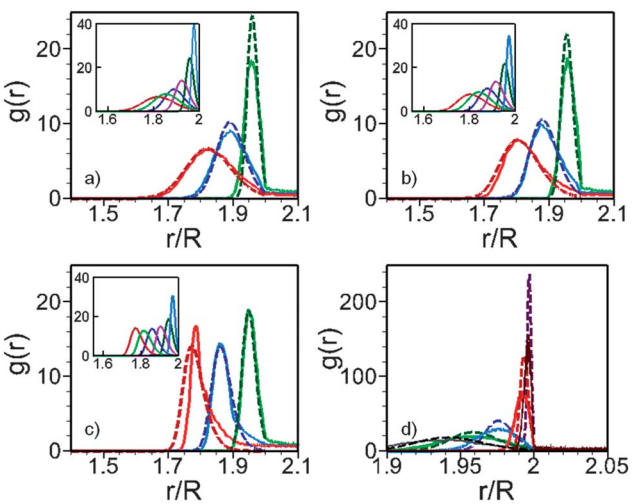

Fig. 5 (Color online) Comparison of theoretical predictions from eqn (5) (dashed lines) of $g(r)$ with computer simulations (solid lines) for a) Hertz potential, b) Compressed emulsions and c) Mooney-Rivlin material. Right to left in a), b) and c): volume fraction =0.7, 0.8 and 0.9. Insets: Theoretical predictions for volume fractions 0.675,0.7,0.75,0.8,0.85 and 0.9 (right to left). d) Hertz potential – volume fractions 0.645, 0.65, 0.675, 0.7, 0.725 (right to left).

The analytical expressions for $a(\phi)$, $g_0(\phi)$ and $\delta(\phi)$determined using the perturbation expansion [eqn (12)–(15)] are plotted as a function of $(\phi - \phi_c)$ in Fig. 6 and are compared with the numerically evaluated values using eqn (5). As expected, $a(\phi)$ and $g_0(\phi)$ diverge while the width $\delta(\phi)$ vanishes as $(\phi \rightarrow \phi_c)$, the hard sphere random close packing limit. The scaling for this behavior in the region $(\phi - \phi_c) = 10^{-3}$ to 10^{-1} are given by

$$a(\phi) \sim (\phi - \phi_c)^{-0.906 \pm 0.0144} \quad (16)$$

$$g_0(\phi) \sim (\phi - \phi_c)^{-0.933 \pm 0.0073} \quad (17)$$

$$\delta(\phi) \sim (\phi - \phi_c)^{0.986 \pm 0.0098} \quad (18)$$

These scalings are close to those derived by Jacquin *et al.*[23] where it was predicted that the peak of $g(r)$, $g_0(\phi) \sim (\phi - \phi_c)^{-1}$and that the width of the peak, $\delta(\phi) \sim (\phi - \phi_c)$. Thus, the theory here predicts closely, the behavior of suspensions near the jamming transition as well as for more compressed suspensions.

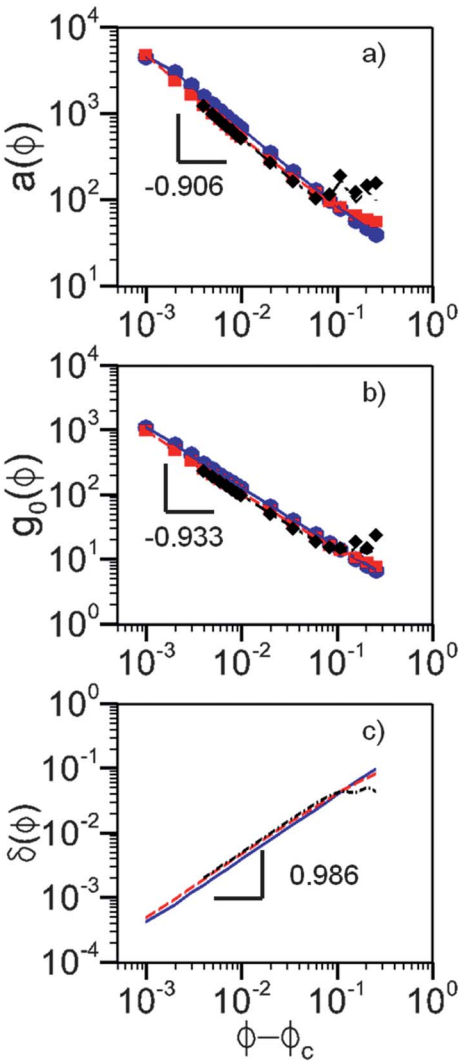

Fig. 6 (Color online) Computational (symbol) and analytic (lines) predictions of $a(\phi)$ and peak and width of $g(r)$ for different volume fractions. (Circles/solid lines – Hertz potential, square/dashed lines –compressed emulsion potential, diamonds/dashed-dotted lines – Mooney-Rivlin potential).

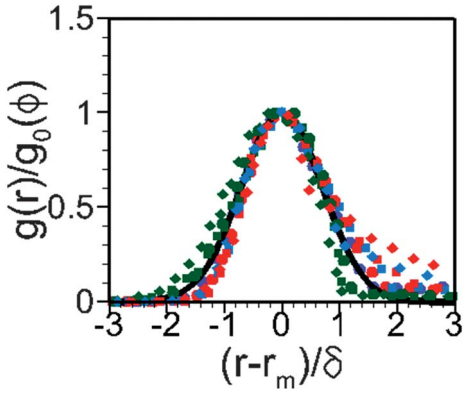

Fig. 7 (Color Online) Theoretical universal curve (black solid line) and scaled simulation data (symbols). Hertz (circles), compressed emulsions (squares) and Mooney-Rivlin materials (diamonds). Volume fractions: 0.65 (green), 0.8 (blue) and 0.9 (red).

From eqn (11), $\frac{g(r)}{g_0(\phi)} = \exp\left[-\left(\frac{r-r_m}{\delta}\right)^2\right]$ is a universal curve for concentrated soft particle suspensions. Fig. 7 shows the theoretical curve (black line) and the scaled simulation data. The simulation data has been scaled with the peak, r_m and width from the simulation results. The agreement is good, especially close to r_m since the Gaussian form has been derived using a quadratic expansion of the potential about r_m.

Elastic properties of these materials can be predicted using $g(r)$. The osmotic pressure and the high frequency elastic modulus can be computed theoretically using eqn (8) and (9). Fig. 8 shows the theoretical predictions of these properties for different interaction potentials as well as predictions from simulations and experimental osmotic pressures for compressed emulsions and foams. The osmotic pressure and elastic moduli for the Hertzian and compressed emulsion potentials appear to approach a plateau value at the higher concentrations. However, for the Mooney-Rivlin material, the bulk materials stiffen with increasing volume fraction and no such plateau is observed. There is good agreement among the theoretical, computational and experimental values.

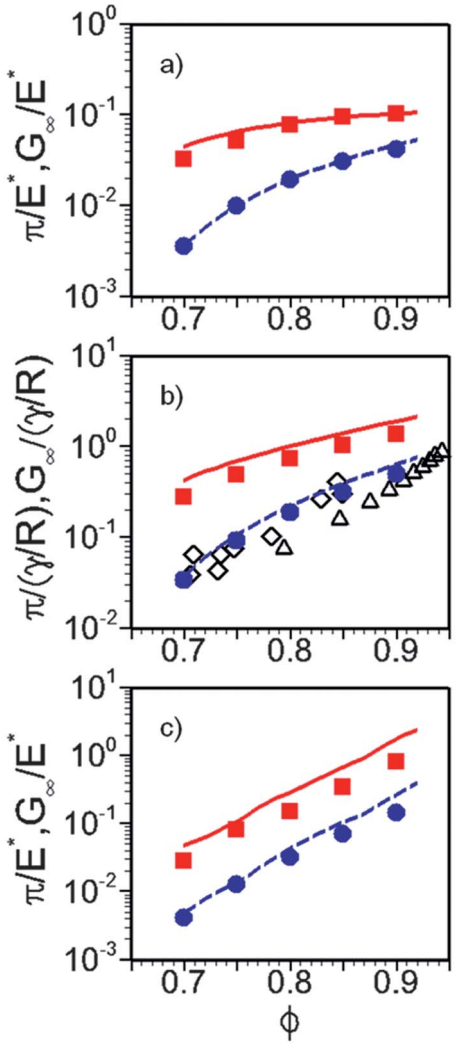

Fig. 8 (Color online) Comparison of theoretical predictions (lines) of elastic properties for a) hertz potential, b) compressed emulsion potential and c) Mooney-Rivlin material potential with computer simulations (circles – osmotic pressure and squares – high frequency modulus) and experiments on osmotic pressure of compressed emulsions (diamond)[10] and foams (triangle).[37] Upper lines: high frequency elastic modulus and lower lines: osmotic pressure.

5. Conclusions

A theory and methodology have been developed to predict the short ranged radial distribution function for athermal, highly concentrated, amorphous suspensions of soft particles based on the transport equation for the distribution function and a component of its flux from a proposed mean elastic force. The theory accurately predicts the distribution function for a variety of soft particles compared to computational simulations. The predicted distribution functions can further be used to accurately predict the osmotic pressure and high frequency modulus. The elastic properties and the radial distribution function g(r) do not change significantly for polydispersities up to 20%.[32] Thus the theory can be used even for mildly polydisperse systems with the average particle radius. Although the main focus of theory is to predict the microstructure and elastic properties at concentrations much larger than random close packing for hard spheres, the predicted radial distribution function becomes singular with the expected scalings as the volume approaches random close packing. This theory provides a new tool for predicting the microstructure for these concentrated soft particle materials.

Acknowledgements

The authors gratefully acknowledge support from National Science Foundation (CBET 0854420) and thank Dr Thomas Truskett for his helpful comments on an earlier version of this paper.

References

1 M. van Hecke, *J. Phys.: Condens. Matter*, 2010, **22**, 033101.
2 R. Borrega, M. Cloitre, I. Betremieux, B. Ernst and L. Leibler, *Europhys. Lett.*, 1999, **47**, 729–735.

3 M. Cloitre, R. Borrega, F. Monti and L. Leibler, *Cr. Phys.*, 2003, **4**, 221–230.
4 S. Fridrikh, C. Raquois, J. F. Tassin and S. Rezaiguia, *J. Chim. Phys. PCB*, 1996, **93**, 941–959.
5 T. G. Mason, J. Bibette and D. A. Weitz, *Phys. Rev. Lett.*, 1995, **75**, 2051–2054.
6 C. N. Likos, *Soft Matter*, 2006, **2**, 478–498.
7 M. Cloitre and R. T. Bonnecaze, *Adv. Polym. Sci.*, 2010, **236**, 117–161.
8 J. R. Seth, L. Mohan, C. Locatelli-Champagne, M. Cloitre and R. T. Bonnecaze, *Nat. Mater.*, 2011, **10**, 838–843.
9 A. Le Grand and G. Petekidis, *Rheol. Acta*, 2008, **47**, 579–590.
10 T. G. Mason, M. D. Lacasse, G. S. Grest, D. Levine, J. Bibette and D. A. Weitz, *Phys. Rev. E: Stat. Phys., Plasmas, Fluids, Relat. Interdiscip. Top.*, 1997, **56**, 3150–3166.
11 R. Zwanzig and R. D. Mountain, *J. Chem. Phys.*, 1965, **43**, 4464–4471.
12 J. P. Hansen and I. R. McDonald, *Theory of Simple Liquids*, Academic Press, 3rd edn, 2006.
13 D. A. McQuarrie, *Statistical Mechanics*, University Science Books, 2000.
14 H. Jacquin and L. Berthier, *Soft Matter*, 2010, **6**, 2970–2974.
15 A. Lang, C. N. Likos, M. Watzlawek and H. Lowen, *J. Phys.: Condens. Matter*, 2000, **12**, 5087–5108.
16 A. A. Louis, P. G. Bolhuis and J. P. Hansen, *Phys. Rev. E: Stat. Phys., Plasmas, Fluids, Relat. Interdiscip. Top.*, 2000, **62**, 7961–7972.
17 M. D. Carbajal-Tinoco, *J. Chem. Phys.*, 2008, **128**, 184507.
18 F. Lado, *Mol. Phys.*, 1984, **52**, 871–876.
19 D. Ben-Amotz and G. Stell, *J. Chem. Phys.*, 2004, **120**, 4844–4851.
20 K. K. Mon, *J. Chem. Phys.*, 2002, **116**, 9392–9394.
21 H. C. Anderson, J. D. Weeks and D. Chandler, *Phys. Rev. A: At., Mol., Opt. Phys.*, 1971, **4**, 1597–1607.
22 G. A. Mansoori and F. B. Canfield, *J. Chem. Phys.*, 1969, **51**, 4958–4967.
23 H. Jacquin, L. Berthier and F. Zamponi, *Phys. Rev. Lett.*, 2011, **106**, 135702.
24 D. Chandler, J. D. Weeks and H. C. Anderson, *Science*, 1983, **220**, 787–794.
25 L. Verlet and J. J. Weis, *Phys. Rev. A: At., Mol., Opt. Phys.*, 1972, **5**, 939–952.
26 J. S. Hoye and A. Reiner, *J. Chem. Phys.*, 2006, **125**, 104503.
27 G. K. Batchelor, *J. Fluid Mech.*, 1977, **83**, 97–117.
28 G. K. Batchelor, *J. Fluid Mech.*, 1976, **74**, 1–29.
29 C. S. O'Hern, L. E. Silbert, A. J. Liu and S. R. Nagel, *Phys. Rev. E: Stat., Nonlinear, Soft Matter Phys.*, 2003, **68**, 011306.
30 C. S. O'Hern, S. A. Langer, A. J. Liu and S. R. Nagel, *Phys. Rev. Lett.*, 2002, **88**, 075507.
31 M. Wyart, L. E. Silbert, S. R. Nagel and T. A. Witten, *Phys. Rev. E: Stat., Nonlinear, Soft Matter Phys.*, 2005, **72**, 051306.
32 J. R. Seth, M. Cloitre and R. T. Bonnecaze, *J. Rheol.*, 2006, **50**, 353–376.
33 B. D. Lubachevsky and F. H. Stillinger, *J. Stat. Phys.*, 1990, **60**, 561–583.
34 K. L. Johnson, *Contact Mechanics*, Cambridge University Press, 1985.
35 M. D. Lacasse, G. S. Grest, D. Levine, T. G. Mason and D. A. Weitz, *Phys. Rev. Lett.*, 1996, **76**, 3448–3451.
36 K. K. Liu, D. R. Williams and B. J. Briscoe, *J. Phys. D: Appl. Phys.*, 1998, **31**, 294–303.
37 H. M. Princen and A. D. Kiss, *Langmuir*, 1987, **3**, 36–41.

